Cancerous object detection using morphological region-based active contour in ultrasound images

Anan Nugroho[1,2*], Risanuri Hidayat [1], Hanung Adi Nugroho[1], Johan Debayle[3]

[1] Department of Electrical & Information Engineering, Universitas Gadjah Mada, Yogyakarta, Indonesia.
[2] Department of Electrical Engineering, Universitas Negeri Semarang, Central Java, Indonesia.
[3] Mines Saint-Etienne, CNRS, UMR 5307 LGF, Centre SPIN, F - 42023 Saint-Etienne, France.

[*]Corresponding author email: anan.sie13@mail.ugm.ac.id; anannugroho@mail.unnes.ac.id

Abstract. Ultrasound is widely utilized in radiological screening to achieve early cancer investigations. Alongside this utilization, the need of object detection and segmentation techniques highly increases as crucial procedure of computer aided diagnosis tool. In addition, the industrial revolution 4.0 also demands automation and digitization in every technological development including computer aided diagnosis systems. This paper presents a morphological region-based active contour called MoRbAC to automatically detect the cancerous objects. Global level set active contour is initially employed to quick segment all objects in the whole image. Inhomogeneity in ultrasound images will lead to erroneous segmentation result. Hence, several morphology operations are taken to enhance it. The cancerous objects are then specifically detected by comparative calculation of area similarity. The proposed MoRbAC was tested in the real ultrasound images of breast and thyroid which validated by manual ground truth localization. Measurements of overlapping and disagreement regions are applied as quantitative indexes to demonstrate its performance. Average values of each validation has achieved i.e accuracy 98.58±0.89%, sensitivity 89.58±7.69%, specificity 99.58±0.11%, precision 95.58±2.77%, similarity 92.36±4.67%. In conclusion, the high performance of MoRbAC indicates its potential for practical applications in ultrasound computer aided diagnosis.

1. Introduction

Currently, we are entering the industrial revolution 4.0 where a technological development cannot be separated from automation, digitization and efficiency [1]. This revolution has penetrated rapidly in various lines of technology including in the modernization of medical imaging. Imaging modalities are playing important role in clinical routine examinations to observe the interior parts of the body. Among them, real time B-mode ultrasound (US) is mostly used to investigate cancerous objects for its low cost, non-invasive, practical and ease of use [2]. Malignancy screening in breast lesions [3] and thyroid nodules [4] is the most prominent US application. However US visual analysis is expert dependent which lead to the high variabilities of interpretation and clinical recommendation. Therefore computer-aided diagnosis (CAD) systems have become a second opinion reader by implementing appropriate image processing algorithms to improve radiologist's diagnoses [5]. Radiologists determine the cancer malignancies according to certain features such as shape, margin, orientation and textural echo pattern of cancerous objects [3]. All of these features can be extracted properly only after the investigated objects are correctly localized. And with the growing abundance of US datasets from continuous screening results, manual localization will be a tiring, tedious and prone to human error. That is why

automated object detection techniques are a key factor in the success of CAD systems [6]. In addition, the enrichment of this capability will make the latest CAD technology survive and compete in the era of industrial revolution 4.0.

Object detection on US images cannot simply be considered as easy work. Low contrast as well as pixel inhomogeneity due to speckles and artifacts make this task challenging [7]. In fact, the high heterogeneity of US often makes cancer findings less distinguishable from surrounding non-cancerous objects. Thus morphological region-based active contour called MoRbAC is proposed to overcome this problem. Region-based active contour refers to a simplified Chan-Vese (CV) level set model [4] that is designed to quickly segment all objects in US images. Models derived from CV are generally insensitive to initialization and independent to image gradient. So that initial contour can be anywhere and the model can responsively detect shapes with or without gradient even for indistinct borders. Moreover binary level set Gaussian filter [8] as regularization term is embedded in it that gives a smoothing effect to maintain stability during evolution. This regularization will also avoid time consuming computation due to reinitialization procedure in standard level set methods.

Basically, the principle of CV is to separate background and foreground based on average intensity values in global manner. This supposition is limited only to homogeneous pixel conditions. Therefore several morphological operations on MoRbAC are carried out to minimize erroneous segmentation results due to the inhomogeneity of US images. With these two stages all objects can be clearly separated from their background even though the targeted cancerous object has not been specifically localized yet. The cancerous objects are then specifically detected by comparative calculation of area similarity. The proposed MoRbAC was tested in the real ultrasound images of breast and thyroid which validated by manual ground truth localization. Several overlapping metrics are presented to demonstrate superiority of MoRbAC. The rest of the paper is structured as follows. Section 2 explains material and methods of MoRbAC framework. Results and discussion are described in Section 3, including MoRbAC's performance and evaluations. Eventually, this paper is concluded in Section 4.

2. Material and Methods

2.1. Radiological ultrasound images

In this study, 4 US sample images of cancerous breast lesions and thyroid nodules were collected from the Department of Radiology, National Central Hospital Sardjito and Air force Central Hospital Hardjolukito Yogyakarta Indonesia. All of them are followed by a manual ground truth according to the radiologist's approval as shown in figure 1. The images are of size around 500 x 650 pixels, which were acquired with 256 gray-level depth using General Electric (GE) and SIEMENS ultrasound machine with linear probe at frequency 7Mhz.

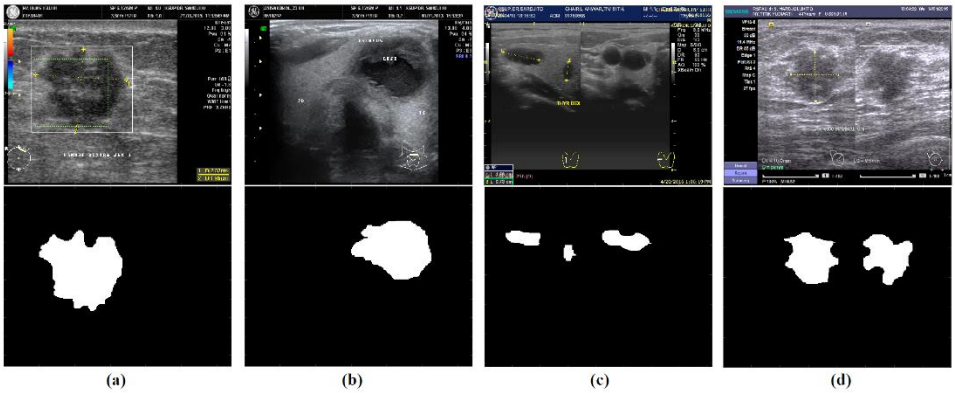

Figure 1. US cancerous objects (a) Single breast lesion, (b) Single thyroid nodule, (c) Triple thyroid nodules, (d) Double breast lesions

2.2. Simplified region-based active contour

Since 'Snakes' was first introduced by Kass et al [9], active contour deformable models have been extensively developed and successfully applied in digital image processing. The basic idea of these models is to dynamically evolve closed curves for image *I(x,y)* in domain Ω so that any existing objects can be detected accurately. Level set theory [10] is generally utilized to represent curve evolution for its capability to handle topological change. The interfacing curve *C* in level set ϕ can be implicitly expressed as

$$\begin{cases} C = (x,y) \in \Omega : \phi(x,y) = 0, \\ inside(C) = (x,y) \in \Omega : \phi(x,y) < 0, \\ outside(C) = (x,y) \in \Omega : \phi(x,y) > 0 \end{cases} \quad (1)$$

Curve evolution is given by zero level set condition at time *t* of the function $\phi(x,y,t)$. Evolving the curve *C* in normal direction with speed *F* follows the differential equation [11] [12]

$$\begin{cases} \phi(x,y,0) = \phi_0(x,y), & \text{for } t = 0 \\ \frac{\partial \phi}{\partial t} = F|\nabla \phi|, & \text{for } t \neq 0 \end{cases} \quad (2)$$

with ∇ is geometric gradient operator, $|\nabla \phi|$ drives the normal direction for contour deformation, and $\{(x,y)|\phi_0(x,y) = 0\}$ denotes the initial level set function. There are two basic models in determining F i.e edge-based geodesic active contour (GAC) [12] and region-based CV [11]. Since GAC just totally depends on edge stopping function performance and the US object boundaries are often indistinct which lead to leakage problem or trapped into local minimal. Besides, GAC also tends to fail in detecting the exterior and interior contours when the initial ϕ_0 is placed far from the investigated object [8]. So far, CV has many advantages compared to GAC. Original CV formulation is given as

$$\frac{\partial \phi}{\partial t} = [\mu . \operatorname{div}\left(\frac{\nabla \phi}{|\nabla \phi|}\right) - \lambda_1 (I - c_1)^2 - \lambda_2 (I - c_2)^2] \delta(\phi) \quad (3)$$

with λ_1, λ_2 and μ are tunable constants. $\delta(\phi)$ is Dirac function which has similar work as $|\nabla \phi|$ [8]. The concept of variational $\delta(\phi)$ [11] is any function that follows

$$\delta(\phi) = \frac{d}{d\phi} H(\phi) \text{ and } H(\phi) = \begin{cases} 1 & \text{if } \phi < 0 \\ 0 & \text{if } \phi > 0 \end{cases} \quad (4)$$

$H(\phi)$ is called Heaviside function, one of which can be formulated with

$$H(\phi) = \frac{1}{\pi} \arctan(\phi) + 0.5 \text{ then } \delta(\phi) = \frac{1}{\pi} \left(\frac{1}{1+\phi^2}\right) \quad (5)$$

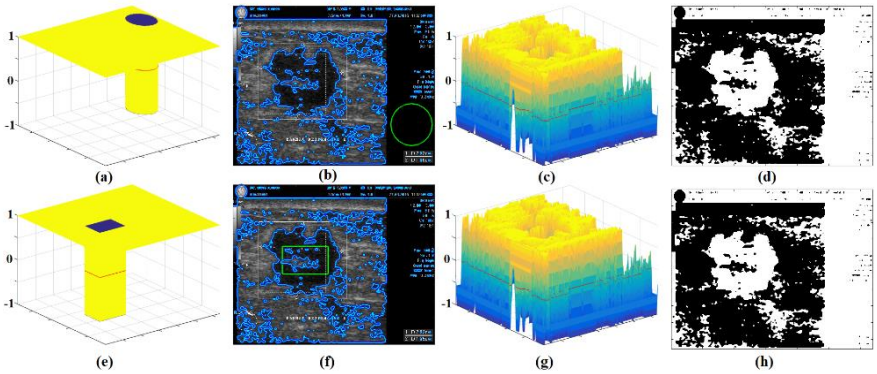

Figure 2. Evolution of CV (a,e) Initial level set function, (b,f) Zero level set of initial (*green*) and final (*cyan*) contour, (c,g) Final level set function, (d,h) Binary representation

whereas c_1, c_2 are average image intensity of inside and outside contour *C* which can be obtained as

$$\begin{cases} c_1(\phi) = \frac{\iint I(x,y).H(\phi)dxdy}{\iint H(\phi)dxdy} & \text{for } \phi < 0 \\ c_2(\phi) = \frac{\iint I(x,y).(1-H(\phi))dxdy}{\iint (1-H(\phi))dxdy} & \text{for } \phi > 0 \end{cases} \quad (6)$$

CV model uses statistical information c_1,c_2 to control evolution and works better on images with weak or borderless edges. Moreover CV is robust of initial contour so that it may be placed anywhere and can still detect both exterior and interior boundaries simultaneously [8]. Figure 2 illustrates it well. However, MoRbAC is designed to work automatically so that any user intervention and manual tuning must be avoided. If we set $\lambda_1 = \lambda_2 = \mu = 1$ and $\delta(\phi)$ is removed, then similar level set evolution can also be obtained with the following model

$$\frac{\partial \phi}{\partial t} = \left(1 - \frac{c_1 + c_2}{2}\right) \quad (7)$$

The main key of CV model is on the mean values of c_1 and c_2. Simplification equation (7) is more beneficial for MoRbAC as it is free of tuning interventions and works faster due to fewer variables involved.

2.3. Level set regularization

Regularization has an important role in maintaining evolution stability in active contour models. Without regularization the level set function will deform irregularly and will be difficult to converge. Thus, evolution goes on for a long time, sometimes even unstoppable. Inspired by Zhang et.al [8], utilizing Gaussian filter on binarized level set is an effectual regularization choice. Important procedures in this regularization technique are as follows:

1. Level set initialization (ϕ_0) by
$$\phi_0 = \phi(x, y, 0) = \begin{cases} -1, & \text{if } (x, y) \in C_0 \\ 1, & \text{otherwise} \end{cases} \quad (8)$$
where C_0 is any closed region in the image domain Ω.
2. Calculate c_1, c_2 using equation (6).
3. Evolve simplifed CV model in equation (7).
4. Binarizing level-set function by let $\phi = 1$ if $\phi > 0$ and $\phi = -1$ elsewhere.
5. Do Gaussian filtering i.e $\phi = \phi * G_\sigma$ where $\sigma = 5$ is a fix deviation kernel.
6. Has the evolution ϕ converged?. If not, return to step 2.

Gaussian filter has a smoothing effect so that evolution of simplified CV is stable and ends with clear results. The binarization procedure will also avoid spiking and flattening of level-set function. Thus level-set evolution converges faster. See figure 3 for illustration.

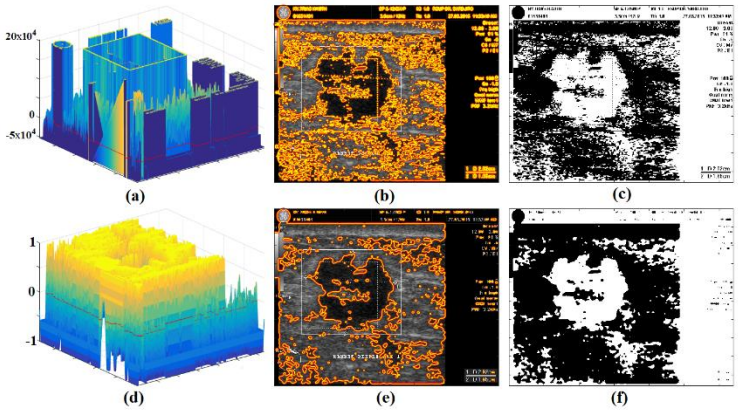

Figure 3. Simplified CV with (*2nd row*) and without (*1st row*) regularization (a,d) Final level set, (b,e) Zero level set contour, (c,f) Binary visualization

2.4. Morphological operations

When the level-set function ϕ has converged, a zero level-set condition can be represented as binary image A by logical operation.

$$A(x,y) = \begin{cases} true, & \text{if } \phi < 0 \\ false, & \text{if } \phi > 0 \end{cases} \tag{9}$$

However, the simplified CV output binary image is less specific. The confounding foregrounds around targeted lesions or nodules complicate object detection. Therefore morphological operations are intended to minimize these undesired foregrounds [13]. First, an opening operation needs to be performed ensuring the cancer objects are separated from the surrounding foreground. If B is a disk structuring element, the opening A_1 is

$$A_1 = A \circ B \tag{10}$$

then border clearing A_2 and filling holes A_3 are two serial steps afterwards

$$A_2 = A_1 \backslash D^i_{A_1}(F_1) \tag{11}$$

$$A_3 = [D^i_{(A_2)^c}(F_1)]^c \tag{12}$$

whereas D is an iterative geodesic dilation that stops at stable condition i [13]

$$D^{(i)}_G(F) = D^{(1)}_G[D^{(i-1)}_G(F)] \tag{13}$$

and

$$D^{(1)}_G(F) = (F \oplus B) \cap G \tag{14}$$

with $D^{(0)}_G(F) = F$. Notations $\oplus$,$\cap$ denote standard dilation and set intersection respectively. G is binary input image called mask and F is binary marker image, where $F \subseteq G$. While F_1 in equation 11, 12 is

$$F_1 = \begin{cases} 1 & if\ on\ the\ border\ of\ I \\ 0 & otherwise \end{cases} \tag{15}$$

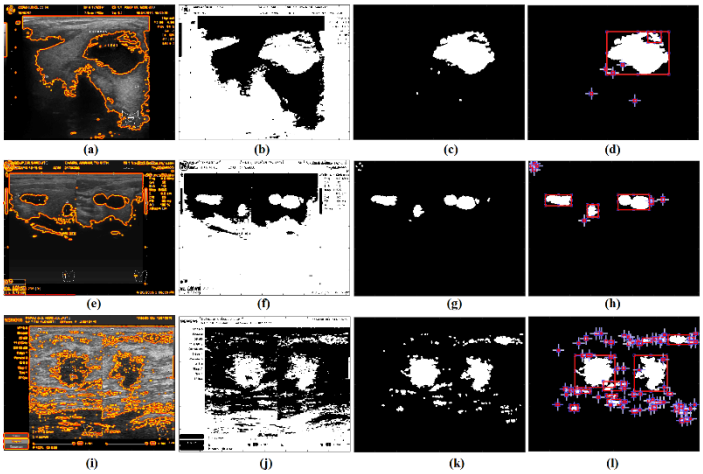

Figure 4. (a,e,i) Simplified CV evolution for other remaining images, (b,f,j) Binary images of each, (c,g,h) Output morphological operations, (d,h,l) Bounding box identification by labeling

The identification of all remaining objects can be obtained using connected component labeling for adjacent foreground pixels [13]. Labeling procedure will produce an image mapping as

$$L(x,y) = \begin{cases} 0 & \text{for } I(x,y) = 0 \\ 1,2,\dots n & \text{for } I(x,y) = 1 \end{cases} \quad (16)$$

I is a binary input image A_3, L is a labeled mapping image and n indicates the number of identified objects. With all foreground labeled, then the area of each object can be obtained at once. Also, the bounding box localization can be created based on the right, left, top and bottom outer pixel information. See figure 4 for more details. Lesions and nodules appear as large foreground areas in ground truth of figure 1. However, cancerous objects are sometimes more than one so that if only based on the largest size, other smaller cancer objects cannot be detected automatically. In fact, the area among cancerous objects in an ultrasound image is not too different. The ratio of smaller to the largest cancerous object is generally more than 70%. If n is the total number of identified foregrounds, R_i is the region area of each, so that

$$\text{Cancerous objects} = \frac{R_i}{\max(R_i)} \geq 0.7 \quad \text{for } i = 1,2,\dots n \quad (17)$$

Thus, non-conformable foregrounds with this constraint are not considered as cancerous objects.

3. Result and Discussion

3.1. The advantages of MoRbAC

In short, MoRbAC is a framework consisting of simplified CV model that is regulated by Gaussian filter and finished with a series of morphological operations for enhancement. Deriving from CV model, MoRbAC is robust against initial contour placement as evidently shown in figure 2. This robustness makes it easy to separate foreground-background in starting object identification as any initialization function can be allowed. Equation 7 has totally eliminated the hassles of manual tuning such as adjusting μ, λ_1, λ_2 in original CV model while maintaining its ability. It can be noted that simplification CV in figure 3(e) is visualized same as the original in figure 2(b,f). The similarity is more noticeable in binary representation between figure 3(f) and figure 2(d,h). Figure 3 also informs that Gaussian filter based regularization is quite effective in suppressing US speckle noise. By this way the final set level evolution becomes more assertive and clean.

Table 1. Computational cost comparison

US images	Iteration number			CPU time (sec)		
	Original CV	Simplified CV non regularization	Simplified CV with regularization	Original CV	Simplified CV non regularization	Simplified CV with regularization
Img1	3	200	3	4.25	48.30	1.78
Img2	4	163	4	3.80	36.34	1.75
Img3	4	60	4	5.64	21.03	2.61
Img4	4	104	4	6.13	35.28	2.58

A notable advantage is found in the comparison of computational costs as reported table 1. The regularized simplification CV can perform as fast as the original model. In fact, much faster in terms of CPU time. Gaussian filter based regularization is reliable in preventing unstoppable level set evolution and ensuring it efficiently converges in low iterations. As detection procedures are carried out in binary images, the morphological operations serve to minimize disturbing foregrounds around targeted objects. Figure 4 shows that cancerous objects of enhanced binary images in the 3rd column are easier recognized

than in 2nd column. And the rightmost column presents bounding box localization based on geometrical extracted features after labeling. The number of localized region of image 1 to 4 are 64,7,10 and 76 foreground respectively. Using equation (17), all of them then can be automatically detected into specific cancerous objects as shown in the 1st row of figure 6.

3.2. Performance of MoRbAC

The MoRbAC's performance was verified by applying it to detect cancerous objects of 4 US images in figure 1. Five overlapping area based metrics were applied to evaluate the results quantitatively [14]. The possibility overlapping regions between bounding box in ground truth and detected object are True Positive (TP), False Positive (FP), False Negative (FN) and True Negative (TN). Figure 4 depicts all these regions.

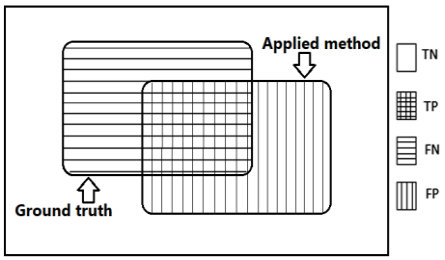

Figure 5. Overlapping area evaluation

Through this overlap definition the five metrics are then formulated as

$$\text{Accuracy} = \frac{|\text{TP+TN}|}{|\text{TP+FP+FN+TN}|} x100 \quad (18)$$

$$\text{Sensitivity} = \frac{|\text{TP}|}{|\text{TP+FN}|} x100 \quad (19)$$

$$\text{Specificity} = \frac{|\text{TN}|}{|\text{TN+FP}|} x100 \quad (20)$$

$$\text{Precision} = \frac{|\text{TP}|}{|\text{TP+FP}|} x100 \quad (21)$$

$$\text{Similarity} = \frac{|2\text{TP}|}{|2\text{TP+FP+FN}|} x100 \quad (22)$$

Achievement values from equation 18 to 22 that are close to 100% indicate the effectiveness of MoRbAC. High performance can be obtained if FP, FN are minimal and leave TP,TN as dominant areas. The 2nd column of figure 6 shows overlapping regions related to all test images. Green squares describe bounding boxes of ground truth while red ones are each detected object. The calculation results of five above metrics are presented in table 2. It can be observed that MoRbAC object detection coincides mostly with its ground truth.

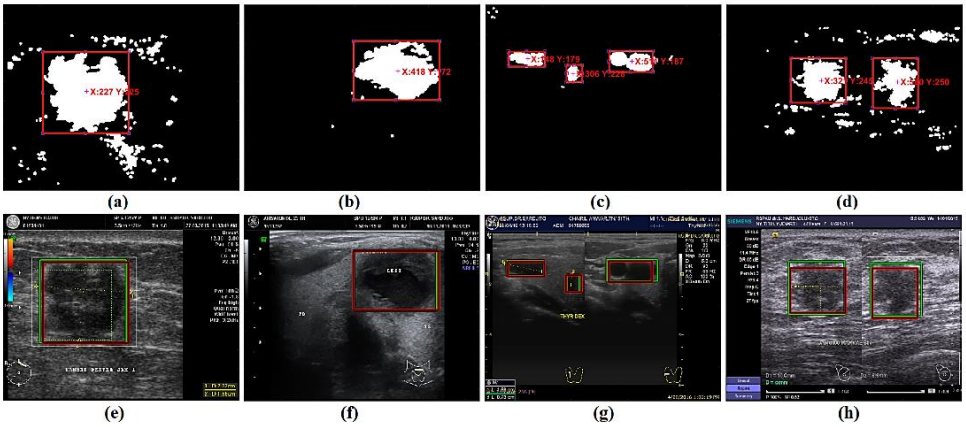

Figure 6. The performance of MoRbAC, (a-d) Detected cancerous objects, (e-h) Overlapping bounding box areas

Table 2. Performance of MoRbAC

Image	Cancerous object	Accuracy (%)	Sensitivity (%)	Specivicity (%)	Precision (%)	Similarity (%)
Img1	1	98.53	93.86	99.43	96.95	95.38
Img2	1	99.39	98.07	99.55	96.55	97.30
Img3	2	97.36	81.56	99.68	97.36	88.76
Img4	3	99.03	84.81	99.65	91.45	88.00

The average performance values of four test images are accuracy 98.58±0.89%, sensitivity 89.58±7.69%, specificity 99.58±0.11%, precision 95.58±2.77% and similarity 92.36±4.67%. Based on this promising performance, MoRbAC is eligible to be used in CAD as automatic detection technique. Worth noting that decisive steps in the CAD procedure are segmentation and feature extraction. Failure in these stages exacerbates clinical recommendations produced by CAD. By localizing each of suspected cancerous objects, these two CAD procedures will be easier to do with accurate result even on an abundant dataset from repeated or continuous US screening.

4. Conclusion

The inevitable industrial revolution 4.0 indirectly requires automation in any CAD system including US imaging applications. Here, the MoRbAC framework contributes to address this challenge. MoRbAC incorporates the advantages of a simplified CV model that is regulated by Gaussian filter and morphological operations for final quality enhancement. Application on real US sample images demonstrates the effectiveness of proposed framework. Developing MoRbAC into a reliable segmentation algorithm is an interesting future work. The US image segmentation process will run fully automatic, fast and accurate for advanced CAD system.

References

[1] A. Petrillo, F. De Felice, R. Cioffi, and F. Zomparelli, "Fourth Industrial Revolution: Current Practices, Challenges, and Opportunities," in *Digital Transformation in Smart Manufacturing*, InTech, 2018
[2] T. L. Szabo, *Diagnostic Ultrasound Imaging: Inside Out*. Elsevier, 2014
[3] A. Rodríguez-Cristerna, W. Gómez-Flores, and W. C. de Albuquerque Pereira, "A computer-aided diagnosis system for breast ultrasound based on weighted BI-RADS classes," *Comput. Methods Programs Biomed.*, vol. 153, pp. 33–40, Jan. 2018
[4] D. Koundal, S. Gupta, and S. Singh, "Computer aided thyroid nodule detection system using medical ultrasound images," *Biomed. Signal Process. Control*, vol. 40, pp. 117–130, Feb. 2018
[5] R. Takahashi and Y. Kajikawa, "Computer-aided diagnosis: A survey with bibliometric analysis," *Int. J. Med. Inform.*, vol. 101, pp. 58–67, May 2017
[6] K. M. Meiburger, U. R. Acharya, and F. Molinari, "Automated localization and segmentation techniques for B-mode ultrasound images: A review," *Comput. Biol. Med.*, vol. 92, pp. 210–235, Jan. 2018
[7] A. Nugroho, R. Hidayat, and H. A. Nugroho, "Artifact removal in radiological ultrasound images using selective and adaptive median filter," in *ACM International Conference Proceeding Series*, 2019
[8] K. Zhang, L. Zhang, H. Song, and W. Zhou, "Active contours with selective local or global segmentation: A new formulation and level set method," *Image Vis. Comput.*, vol. 28, no. 4,pp. 668–676, Apr. 2010
[9] M. Kass, A. Witkin, and D. Terzopoulos, "Snakes: Active contour models," *Int. J. Comput.*

Vis., vol. 1, no. 4, pp. 321–331, Jan. 1988
[10] S. Osher and J. A. Sethian, "Fronts propagating with curvature-dependent speed: Algorithms based on Hamilton-Jacobi formulations," *J. Comput. Phys.*, vol. 79, no. 1, pp. 12–49, Nov. 1988
[11] T. F. Chan and L. A. Vese, "Active contours without edges," *IEEE Trans. Image Process.*, vol. 10, no. 2, pp. 266–277, 2001
[12] V. Caselles, R. Kimmel, and G. Sapiro, "Geodesic Active Contours," *Int. J. Comput. Vis.*,1997.
[13] P. Soille, *Morphological Image Analysis : Principles and Applications*. 2004
[14] J. Shan, H. D. Cheng, and Y. Wang, "A novel segmentation method for breast ultrasound images based on neutrosophic l-means clustering," *Med. Phys.*, vol. 39, no. 9, pp. 5669–5682, Aug. 2012

Acknowledgments
This work is funded by Department of Electrical Engineering, Universitas Negeri Semarang. The authors would also like to thank Dr. Lina Choridah, Sp.Rad and her mentored students in the Department of Radiology, Faculty of Medicine, Universitas Gadjah Mada for related radiological US images including their ground truth.